Charge Order in $LuFe_2O_4$: An Unlikely Route to Ferroelectricity

J. de Groot,[1] T. Mueller,[1] R. A. Rosenberg,[2] D. J. Keavney,[2] Z. Islam,[2] J.-W. Kim,[2] and M. Angst[1,*]

[1]*Peter Grünberg Institut PGI and Jülich Centre for Neutron Science JCNS, JARA-FIT, Forschungszentrum Jülich GmbH, 52425 Jülich, Germany*

[2]*Argonne National Laboratory, 9700 S. Cass Avenue, Argonne, Illinois 60439, USA*

(Received 5 December 2011; published 1 May 2012)

We present the refinement of the crystal structure of charge-ordered $LuFe_2O_4$, based on single-crystal x-ray diffraction data. The arrangement of the different Fe-valence states, determined with bond-valence-sum analysis, corresponds to a stacking of charged Fe bilayers, in contrast with the polar bilayers previously suggested. This arrangement is supported by an analysis of x-ray magnetic circular dichroism spectra, which also evidences a strong charge-spin coupling. The nonpolar bilayers are inconsistent with charge order based ferroelectricity.

DOI: 10.1103/PhysRevLett.108.187601 PACS numbers: 77.84.−s, 61.05.cf, 75.50.Gg, 78.70.Dm

Multiferroic oxides with strong magnetoelectric coupling are of high interest for potential information-technology applications [1], but they are rare because the traditional mechanism of ferroelectricity is incompatible with magnetism [2]. Consequently, much attention is focused on various unconventional mechanisms of ferroelectricity [1]. Of these, ferroelectricity originating from charge ordering (CO) is particularly intriguing because it potentially combines large electric polarizations with strong magnetoelectric coupling [3]. However, examples of oxides where this mechanism occurs are exceedingly rare and none is really well understood.

$LuFe_2O_4$ is often cited as the prototypical example of CO-based ferroelectricity (see, e.g., [1]). In this material, the Fe-valence order has been proposed to render the triangular Fe/O bilayers [see Fig. 1(a)] polar by making one of the two layers rich in Fe^{2+} and the other in Fe^{3+} [4]. Because of this new mechanism of ferroelectricity and also because of the high transition temperatures of CO ($T_{CO} \sim 320$ K) and magnetism ($T_N \sim 240$ K), $LuFe_2O_4$ is increasingly attracting attention [5–25]. That the Fe/O bilayers become polar upon CO has never been challenged. Symmetry analysis of CO superstructure reflections [20] led to the proposal of an antiferroelectric stacking of the bilayer polarizations in the ground state, but did not cast into doubt the polar nature of the CO bilayers. Although these polar bilayers are generally accepted in the $LuFe_2O_4$ literature [5–10], a direct proof is lacking. An assumption-free experimental determination of whether or not the CO in the Fe/O bilayers is polar would be crucial given the dependence of the proposed mechanism of ferroelectricity in $LuFe_2O_4$ on polar bilayers.

In this Letter, we present the first crystal structural refinement taking into account the superstructure due to CO in $LuFe_2O_4$, performed on single-crystal x-ray diffraction data. Identifying the positions of Fe^{2+} and Fe^{3+} valences in the structure with the bond-valence-sum (BVS) analysis, an unexpected new CO pattern with charged Fe/O bilayers emerges [Fig. 1(a)]. We also present x-ray magnetic circular dichroism (XMCD) measurements, which link [Fig. 1(a)] the CO with the spin order determined elsewhere [23], further corroborating the new CO pattern. This new CO arrangement with charged and *nonpolar* bilayers is in strong contrast to all previously suggested CO configurations with polar bilayers [4,20,26]. We discuss the implications of this result on "*ferroelectricity from CO*" in $LuFe_2O_4$, addressing the possibility of polarizing the bilayers by an electric field. Finally, we also address the relevance of the strict spin-charge coupling to the CO transition.

Laboratory x-ray diffraction work was done on well-characterized crystals with an Agilent-Technologies

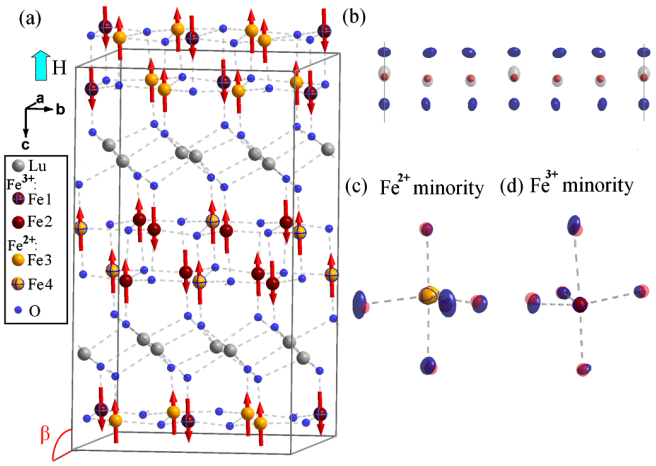

FIG. 1 (color online). (a) Monoclinic crystal structure $C2/m$ of $LuFe_2O_4$ ($a = 5.95$ Å, $b = 10.30$ Å, $c = 16.96$ Å, $\beta = 96.72°$). The refined data were measured at 210 K. The ferrimagnetic high-field spin order and $Fe^{3+/2+}$ charge order is represented by arrows and different colors, respectively. (b) Lu and O atoms drawn as thermal ellipsoids in the projection along a. For comparison, the Lu positions at 350 K are displayed as spheres. (c), (d) O coordination at 210 K and 350 K for the $Fe^{2+/3+}$ minority (small spheres indicate the O positions at 350 K).

SuperNova diffractometer using Mo-K_α radiation and a cryojet HT for temperature control. Above T_{CO} (at 350 K) the crystal structure of $LuFe_2O_4$ was refined [27] in $R\bar{3}m$ symmetry, with similar results as [28] and a low R factor $R[F^2 > 4\sigma(F^2)] = 1.87\%$. As already reported in [20,26,29], by cooling through T_{CO} strong diffuse scattering along $(\frac{1}{3}\,\frac{1}{3}\,\ell)$ splits into sharp CO superstructure reflections [Fig. 2(a) and 2(b)], with a small incomensurability. Only samples showing the best magnetic behavior, corresponding to those studied in [20–24], show these sharp superstructure peaks already at room temperature. For refinements, the apparent small incommensuration away from $(\frac{1}{3}\,\frac{1}{3}\,\ell)$ and $(00\,\frac{3}{2})$ type reflections was neglected, because it most likely corresponds, not to a "truly incommensurate" structure [30], but rather to a discommensuration from anti-phase boundaries as previously proposed for $LuFe_2O_4$ [20,26] and also observed in other CO oxides [31]. The superstructure reflections originate from three individual CO domains [20] corresponding to 120° twinning with $(\frac{1}{3}\,\frac{1}{3}\,\frac{3}{2})$ and symmetry-equivalent $(\frac{1}{3}\,\frac{2}{3}\,\frac{3}{2})$ and $(\frac{2}{3}\,\frac{1}{3}\,\frac{3}{2})$ propagation vectors, as illustrated in Fig. 1 of [22].

From a symmetry analysis in the hexagonal cell with $(\frac{1}{3}\,\frac{1}{3}\,\frac{3}{2})$ propagation, two irreducible representations are allowed, both of which lower the space group to $C2/m$. These correspond to different origin positions (centers of inversion) of the monoclinic cell. In one case, it is located at the Lu positions between the bilayers; this structure corresponds to antiferroelectrically stacked polar bilayers, as proposed in [20]. For the other case, the inversion center is located between the two Fe layers of a bilayer, corresponding to (nonpolar) bilayers with a net charge. This latter case was appraised as unlikely due to the necessity of interbilayer charge transfer [20]. However, only a full structural refinement can decide which representation is actually realized. A consequence from the domain structure is that some reflections totally overlap in reciprocal space, while others are difficult to separate, making a reliable refinement difficult.

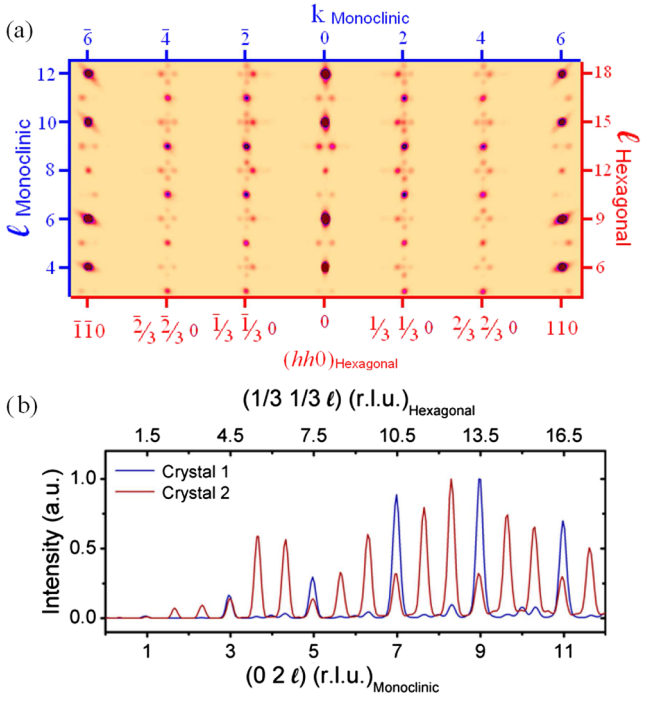

FIG. 2 (color online). (a) Composite precession image of crystal 1 in the $(0k\ell)_{Mon}$ plane indexed in the new monoclinic cell, measured at 210 K. (b) Intensity distribution along $(02\ell)_{Mon}$ for two crystals at 210 K.

Therefore, a quantity of small crystals, obtained from one crushed sample from the same batch as in [20–24] showing the best magnetic behavior [23], was screened for their domain populations. In all experiments, the three domains were readily identified by the diffractometer software as twinned monoclinic cells with $C2/m$ symmetry. Most crystals show near-equilibrium populations [e.g., crystal 2 in Fig. 2(b)], but some are close to a single-domain state (ratios of 0.03:0.09:1 for crystal 1), alleviating the structural refinement. On this crystal we collected 8556 reflections (1285 unique); all intensities were corrected by numerical absorption correction using indexed crystal faces.

A refinement in the structure model with the center of inversion located in the Lu layers, corresponding to the representation with antiferroelectrically stacked bilayers [20], led to very anisotropic displacement parameters for Lu along the c_{Hex} direction. This is very unlikely for the heavy Lu ions. A relatively poor agreement was achieved: $R[F^2 > 4\sigma(F^2)] \sim 15\%$.

For refinements corresponding to the second representation with the center of inversion between the bilayers, a much better $R[F^2 > 4\sigma(F^2)] = 5.96\%$ is achieved. Additional refinements in lower-symmetry space groups, e.g., Cm, allowing for both CO configurations, reproduces a structure very close to this second, with only marginally improved R values. This makes a lower symmetry than $C2/m$ very unlikely. The $C2/m$ structural solution is presented in Fig. 1(a) [32]. At 210 K a Lu distortion along c_{Hex} with an amplitude of ~0.14 Å [see Fig. 1(b)] is clearly connected to the $Fe^{2+/3+}$ CO involving O shifts on the Fe-O-Lu path, explaining the poor refinement with large anisotropic displacement parameters for Lu on high-symmetry sites (also visible as precursor effect in the hexagonal solution above T_{CO} [28,32]). For different Fe sites, strong deviations for the positions of surrounding O atoms with respect to the high-T structure are visible in Figs. 1(c) and 1(d), indicating a separation into two Fe-valence states according to the average Fe-O bond lengths (Table I). For Fe^{2+} and Fe^{3+} the average Fe-O bond length in a trigonal bipyramidal coordination should be 2.09 Å and 1.98 Å, respectively [33].

To determine the valence V from different cation sites a BVS analysis [34] was performed: $V = \sum_i \exp[(d_0 - d_i)/0.37]$. Here, d_i are the experimental

TABLE I. Valences from the bond-valence-sum for different Fe sites at 210 K [$C2/m$] and 350 K [$R\bar{3}m$].

Site	T[K]	⟨(Fe-O)⟩[Å]	V from BVS	Wyckoff
$Fe_{R\bar{3}m}$	350	2.030	2.38(3)	6c
Fe1	210	1.998	2.91(2)	4i
Fe2	210	1.999	2.75(2)	8j
Fe3	210	2.058	2.10(1)	8j
Fe4	210	2.100	1.92(1)	4i

bond lengths to the surrounding ions and d_0 is a tabulated empirical value characteristic for the cation-anion pair [34]. The Lu valences from BVS calculations are very close to 3+ for all temperatures and sites. The results for the Fe sites are shown in Table I and illustrated by different shadings for different Fe sites in Fig. 1 for the CO phase. The temperature dependence of the BVS [Fig. 3(a)] indicates below T_{CO} an increasing valence separation upon cooling, with a plateau reached below 260 K. At $T_{LT} \sim$ 170 K there is a magneto-structural phase transition with a small splitting of structural reflections [21]. For the data at 120 K an abnormal increase of the c_{Hex}, calculated from the monoclinic lattice, is observed. However, in the refinements only very subtle changes of atom positions are achieved, not affecting the CO configuration (120 K in Fig. 3) from BVS calculations, or the $C2/m$ symmetry.

The Fe-valence separation on majority sites tends to be smaller than for the minority sites. The average valence of all Fe sites from BVS is ~2.4, the same as the Fe-BVS above T_{CO}, suggesting nonperfect ionicity of the bonds to the O despite of the large valence separation. The latter is also supported by a recent resonant x-ray diffraction study [25], in which a full 2+/3+ valence separation was deduced from the chemical shifts of the Fe K edge. The valence separation deduced from BVS analysis is considerably larger than that for other CO Fe oxides, except for Fe_2OBO_3 [35].

Is the new CO arrangement presented here consistent with the magnetic structure presented in [23]? Are the magnetic structures predetermined by the CO? The x-ray magnetic circular dichroism (XMCD) at the Fe L edges is the ideal tool to address these questions. Two previous XMCD studies on $LuFe_2O_4$ were reported [7,13,36], but both were performed on samples for which no long-range charge and magnetic order has been demonstrated. To test whether the strong spin-charge coupling deduced in [7,13] also applies to samples exhibiting long-range spin and CO, we performed XMCD at the beam line 4-ID-C of the Advanced Photon Source (APS). We used magnetic fields up to 4 T$||c_{Hex}$ and the incoming beam and the total electron yield as x-ray absorption spectra (XAS). The total fluorescence yield signal (30° between k_i and c_{Hex}) is dominated by reabsorption, but confirms the bulk nature of our XMCD [37]. The XMCD signal was then calculated from the difference between the XAS (from the total electron yield) for positive and negative circular polarization (μ_+ and μ_-), with no nonmagnetic XMCD contributions [37]. To see if there is any change in the CO configuration or structure between the two magnetic phases, we have done additional high-resolution x-ray diffraction at the beam line 6-ID-D (APS) above T_{LT}. The diffraction data in $H||c_{Hex}$ up to 2.5 T, show neither a change in the CO configuration nor a structural transition.

In the high-field ferrimagnetic phase [23], the shape of the XMCD spectra $\Delta\mu$ [Fig. 3(b)] is similar to the ones shown in [7,13]. With the sum rule [38,39], we could extract from the integrated dichroism $\Sigma(\Delta\mu)$ a similar orbital-to-spin moment ratio of ~0.3 corresponding to an orbital magnetic moment of $\sim 0.7\mu_B$/f.u., as previously reported [38,39]. This observed unquenched orbital moment excludes the possibility of Fe^{2+} orbital order for the ferrimagnetic phase; orbital order would imply a lifting of the two-fold-degeneracy of the lowest crystal-field doublet, which is occupied by a minority spin. However, this degeneracy is necessary for an orbital magnetic moment [40]. For the antiferro- and paramagnetic phases it can also be excluded, indirectly, because there is no structural component in the transitions involved. Because of the structural transition at T_{LT} [21] we can not exclude long-range orbital

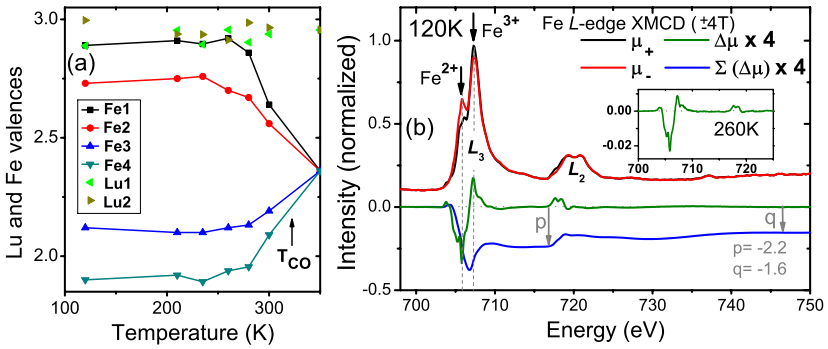

FIG. 3 (color online). (a) Fe and Lu valence states for different sites from the bond-valence-sum method. (b) XMCD spectra across the Fe $L_{2/3}$ edge at 120 K and 260 K (inset). The XAS spectra with H parallel and antiparallel to the incoming beam by changed photon polarization were averaged by subtracting them from each other [37].

order in this low temperature phase, which could be consistent with the observed lattice parameter changes. However, a detailed discussion is beyond the scope of the present study.

Two prominent peaks in the L_3 region of the XAS are readily identified as the chemically shifted Fe^{2+} and Fe^{3+} white lines [7,13]. In the XMCD spectra the large downward peak at the Fe^{2+} position and smaller upward peak at the Fe^{3+} position, directly imply that the net moment of Fe^{2+} is in the field direction and a smaller net moment of the Fe^{3+} sites points opposite to the field. For the local $Fe^{2+/3+}$ spin configurations, the model of [7,13], extracted from a similar XMCD shape, together with the CO presented here, is consistent with the ferrimagnetic spinstructure of [23].

More important, the above implications of the XMCD signal, combined with the ferrimagnetic model [23], verify the novel CO configuration. Given the absence of partial disorder, only three valence specific local spin configurations are possible, of which only one is consistent with the overall magnetic saturation moment of $\sim 3\mu_B$/f.u. [37]: All Fe^{2+} as well as $\frac{1}{3}$ of the Fe^{3+} spins are aligned in the H direction, $\frac{2}{3}$ of the Fe^{3+} spins point opposite to H, the same model as proposed in [7,13]. Combining this local spin-charge configuration with the ferrimagnetic spin order [23] directly excludes any (anti)ferroelectric model preserving mirror symmetry. Ignoring mirror symmetry, 28 configurations are possible [41], of which, however, only the one presented in Fig. 1(a) fits to the right intensity distribution along the $(02\ell)_{\mathrm{Mon}}$ line [Fig. 2(b)]; this is also the only one of the 28 preserving mirror symmetry.

Furthermore, as discussed in [23] the refinement of spin structures can be improved by introducing different magnetic moments for Fe^{2+} and Fe^{3+} according to the charged-bilayer CO model, which is not the case for any CO with polar bilayers. This also supports the above analysis, though by itself the weight of this evidence is reduced by a similar improvement of the refinement regarding a possible magnetic contamination.

Thus, structure refinement, XMCD, and magnetic contrast, all clearly identify the CO configuration with charged bilayers [Fig. 1(a)] as the correct one. This charge pattern is very surprising, because it requires interbilayer charge transfer. For this reason it was considered before only in [20], where it was mentioned as symmetry allowed but excluded as physically unlikely. Understanding the origin of this long-range (~ 6 Å) charge transfer calls for further theoretical work.

Importantly, this new CO structure does not contain polar bilayers, in contrast to what was previously proposed (e.g., [4,20]), casting doubt on the ''ferroelectricity from charge ordering'' scenario. How general is our result, given the significant reported (see, e.g., [12]) sample-to-sample variations? Clearly, the structure refinement can be expected to be representative for all samples where ($\frac{1}{3}$, $\frac{1}{3}$, half-integer) reflections are observed as main CO order parameter (e.g., [4,5,18,20–26,29]), the similarity of observed XMCD spectra with [7,13] even suggests that the same basic CO configuration also applies to samples without long-range CO (e.g., [14]). In particular, our refinement should be valid for the samples on which pyroelectric current measurements have been reported [4].

To explain the pyroelectric current measurements, some of us proposed [20] that a ferroelectric CO might be stabilized by an electric field, though such a scenario seems less likely when charged bilayers have to be polarized. Indeed, a CO remaining completely robust in electric fields has been reported by Wen *et al.* [18], based on neutron diffraction. We have confirmed this as also valid for our samples by additional x-ray diffraction measurements in electric fields up to 15 kV cm^{-1} at APS 6-ID-D and 6-ID-B, and thus conclude that a ferroelectric CO cannot be stabilized by electric fields.

The relatively low resistivity around T_{CO} [15–19] could provide an alternative explanation for the pyroelectric current measurements of [4], because in the presence of residual conductivity nonferroelectrics can exhibit currents strongly resembling ferroelectric depolarization currents, due to space-charge effects [42]. The also observed [4,43] giant dielectric constants could be attributed to interface effects [19]. All reported macroscopic indications of ferroelectric behavior in $LuFe_2O_4$ are therefore most likely due to extrinsic effects.

Returning to XMCD, the analysis not only shows the consistency of the new CO and the spin order, but also implies a strict coupling of these orders. Interestingly, XMCD spectra taken above T_N in ± 4 T [Fig. 3(b) inset] have a small amplitude, but indicate the same $Fe^{2+/3+}$ spin configuration as in the ferrimagnetic phase. This is consistent with the conclusion for $H = 0$ of randomly stacked bilayers that are still individually magnetically ordered based on diffuse magnetic scattering [23]: Partial polarization by a magnetic field is then expected to lead to the same relative net moments on Fe^{2+} and Fe^{3+}, provided the spin-charge coupling remains. This signifies still ordered Fe bilayers in the paramagnetic phase with strictly coupled charge and spin order persisting well above T_N, from susceptibility also likely above T_{CO}. This suggests at high T short-range precursors with already coupled local spin and CO. This coupling already above T_{CO} is most likely the origin of the magnetic-field control of the charge structures reported in [8].

In conclusion, crystal structure refinements of charge-ordered $LuFe_2O_4$ show that the Fe/O bilayers are charged rather than polar. This is further supported by an analysis of XMCD data, which also indicates a strict spin-charge coupling extending to the fluctuations regime above the ordering temperature. The nonpolar CO, which is not affected by electric fields, precludes CO-based ferroelectricity in $LuFe_2O_4$. Hence, a clear example of an oxide

material with ferroelectricity originating from CO has yet to be identified.

We gratefully acknowledge D. Robinson for help with collecting data. Support from the initiative and networking fund of the Helmholtz Association of German Research Centers by funding the Helmholz-University Young Investigator Group "Complex Ordering Phenomena in Multifunctional Oxides," is gratefully acknowledged. Use of the Advance Photon Source was supported by the U.S. Department of Energy, Office of Science, Office of Basic Energy Sciences, under Contract No. DE-AC02-06CH11357. M. A. thanks D. Mandrus, B. C. Sales, W. Tian, and R. Jin for their assistance in crystal growth, also supported by the U.S. DOE.

*M.Angst@fz-juelich.de

[1] K. F. Wang, J.-M. Liu, and Z. F. Ren, Adv. Phys. **58**, 321 (2009).
[2] N. A. Hill, J. Phys. Chem. B **104**, 6694 (2000).
[3] J. van den Brink and D. I. Khomskii, J. Phys. Condens. Matter **20**, 434217 (2008).
[4] N. Ikeda *et al.*, Nature (London) **436**, 1136 (2005).
[5] A. M. Mulders, M. Bartkowiak, J. R. Hester, E. Pomjakushina, and K. Conder, Phys. Rev. B **84**, 140403 (R) (2011).
[6] A. B. Harris and T. Yildirim, Phys. Rev. B **81**, 134417 (2010).
[7] K.-T. Ko, H.-J. Noh, J.-Y. Kim, B.-G. Park, J.-H. Park, A. Tanaka, S. B. Kim, C. L. Zhang, and S-W. Cheong, Phys. Rev. Lett. **103**, 207202 (2009).
[8] J. Wen, G. Xu, G. Gu, and S. M. Shapiro, Phys. Rev. B **80**, 020403(R) (2009).
[9] H. J. Xiang and M.-H. Whangbo, Phys. Rev. Lett. **98**, 246403 (2007).
[10] A. Nagano, M. Naka, J. Nasu, and S. Ishihara, Phys. Rev. Lett. **99**, 217202 (2007).
[11] J. Rouquette *et al.*, Phys. Rev. Lett. **105**, 237203 (2010).
[12] T. Michiuchi *et al.*, Ferroelectrics **378**, 175 (2009).
[13] K. Kuepper *et al.*, Phys. Rev. B **80**, 220409(R) (2009).
[14] W. Wu *et al.*, Phys. Rev. Lett. **101**, 137203 (2008).
[15] L. J. Zeng, H. X. Yang, Y. Zhang, H. F. Tian, C. Ma, Y. B. Qin, Y. G. Zhao, and J. Q. Li, Europhys. Lett. **84**, 57011 (2008).
[16] C. Li, X. Zhang, Z. Cheng, and Y. Sun, Appl. Phys. Lett. **93**, 152103 (2008).
[17] B. Fisher, J. Genossar, L. Patlagan, and G. M. Reisner, J. Appl. Phys. **109**, 084111 (2011).
[18] J. Wen, G. Xu, G. Gu, and S. M. Shapiro, Phys. Rev. B **81**, 144121 (2010).
[19] P. Ren, Z. Yang, W. G. Zhu, C. H. A. Huan, and L. Wang, J. Appl. Phys. **109**, 074109 (2011); D. Niermann, F. Waschkowski, J. de Groot, M. Angst, and J. Hemberger, arXiv:1203.1200v1.
[20] M. Angst *et al.*, Phys. Rev. Lett. **101**, 227601 (2008).
[21] X. S. Xu *et al.*, Phys. Rev. Lett. **101**, 227602 (2008).
[22] X. S. Xu, J. de Groot, Q.-C. Sun, B. C. Sales, D. Mandrus, M. Angst, A. P. Litvinchuk, and J. L. Musfeldt, Phys. Rev. B **82**, 014304 (2010).
[23] J. de Groot *et al.*, Phys. Rev. Lett. **108**, 037206 (2012).
[24] A. D. Christianson *et al.*, Phys. Rev. Lett. **100**, 107601 (2008).
[25] A. M. Mulders, S. M. Lawrence, U. Staub, M. Garcia-Fernandez, V. Scagnoli, C. Mazzoli, E. Pomjakushina, K. Conder, and Y. Wang, Phys. Rev. Lett. **103**, 077602 (2009).
[26] Y. Yamada, S. Nohdo, and N. Ikeda, J. Phys. Soc. Jpn. **66**, 3733 (1997).
[27] L. J. Farrugia, J. Appl. Crystallogr. **32**, 837 (1999).
[28] M. Isobe, N. Kimizuka, J. Iida, and S. Takekawa, Acta Crystallogr. Sect. C **46**, 1917 (1990).
[29] Y. Yamada, K. Kitsuda, S. Nohdo, and N. Ikeda, Phys. Rev. B **62**, 12167 (2000).
[30] H. J. Kim, C. D. Malliakas, A. T. Tomić, S. H. Tessmer, M. G. Kanatzidis, and S. J. L. Billinge, Phys. Rev. Lett. **96**, 226401 (2006).
[31] M. Angst *et al.*, Phys. Rev. Lett. **99**, 256402 (2007).
[32] The structures refined are deposited in the Inorganic Crystal Structure Database with access numbers: 423 570, 423 569 (350 K and 210 K).
[33] R. D. Shannon, Acta Crystallogr. Sect. A **32**, 751 (1976).
[34] N. E. Brese and M. O'Keeffe, Acta Crystallogr. Sect. B **47**, 192 (1991); I. D. Brown, *The Chemical Bond in Inorganic Chemistry: The Bond Valence Model* (Oxford University Press, Oxford, 2002).
[35] M. Angst, P. Khalifah, R. P. Hermann, H. J. Xiang, M.-H. Whangbo, V. Varadarajan, J. W. Brill, B. C. Sales, and D. Mandrus, Phys. Rev. Lett. **99**, 086403 (2007).
[36] In addition, there is an XMCD study on substitutioned compounds: H.-J. Noh, H. Sung, J. Jeong, J. Jeong, S. B. Kim, J.-Y. Kim, J. Y. Kim, and B. K. Cho, Phys. Rev. B **82**, 024423 (2010).
[37] See Supplemental Material at http://link.aps.org/supplemental/10.1103/PhysRevLett.108.187601 for more details concerning the XMCD spectra.
[38] B. T. Thole, P. Carra, F. Sette, and G. van der Laan, Phys. Rev. Lett. **68**, 1943 (1992).
[39] C. T. Chen, Y. U. Idzerda, H.-J. Lin, N. V. Smith, G. Meigs, E. Chaban, G. H. Ho, E. Pellegrin, and F. Sette, Phys. Rev. Lett. **75**, 152 (1995).
[40] I. B. Bersuker, *Electronic Structure and Properties of Transition Metal Compounds* (John Wiley & Sons, Inc., New Jersey, 2012), 2nd ed..
[41] All four $\downarrow$ sites must be Fe^{3+}, and the number of possibilities to distribute the two remaining Fe^{3+} among the 8 $\uparrow$ sites is $\binom{8}{2} = 28$.
[42] M. Maglione and M. A. Subramanian, Appl. Phys. Lett. **93**, 032902 (2008).
[43] M. A. Subramanian, T. He, J. Chen, N. S. Rogado, T. G. Calvarese, and A. W. Sleight, Adv. Mater. **18**, 1737 (2006).